J Physiol 587.4 (2009) pp 745–752

The Journal of Physiology

RAPID REPORT

Rapid and local autoregulation of cerebrovascular blood flow: a deep-brain imaging study in the mouse

Nahoko Kuga[1], Tadashi Hirata[2], Ikuko Sakai[2], Yoshihisa Tanikawa[3], Huei Yu Chiou[1], Takuma Kitanishi[1], Norio Matsuki[1] and Yuji Ikegaya[1,4]

[1] *Laboratory of Chemical Pharmacology, Graduate School of Pharmaceutical Sciences, The University of Tokyo, 7-3-1 Hongo, Bunkyo-ku, Tokyo 113-0033, Japan*
[2] *Advanced Core Technology Department, Research and Development Division, Olympus Corporation, 2-3 Kuboyama-cho, Hachioji-shi, Tokyo 192-8512, Japan*
[3] *Product Development Department II, Micro-Imaging Systems Division, Olympus Corporation, 2951 ishikawa-cho, Hachioji-shi, Tokyo 192-8507, Japan*
[4] *Precursory Research for Embryonic Science and Technology (PRESTO), Japan Science and Technology Agency, 5 Sanbancho Chiyoda-ku, Tokyo 102-0075, Japan*

The brain obtains energy by keeping the cerebral blood flow constant against unexpected changes in systemic blood pressure. Although this homeostatic mechanism is widely known as cerebrovascular autoregulation, it is not understood how widely and how robustly it works in the brain. Using a needle-like objective lens designed for deep-tissue imaging, we quantified the degree of autoregulation in the mouse hippocampus with single-capillary resolution. On average, hippocampal blood flow exhibited autoregulation over a comparatively broad range of arterial blood pressure and did not significantly respond to pressure changes induced by the pharmacological activation of autonomic nervous system receptors, whereas peripheral tissues showed linear blood flow changes. At the level of individual capillaries, however, about 40% of hippocampal capillaries did not undergo rapid autoregulation. This heterogeneity suggests the presence of a local baroreflex system to implement cerebral autoregulation.

(Received 11 September 2008; accepted after revision 9 December 2008; first published online 15 December 2008)
Corresponding author Y. Ikegaya: Laboratory of Chemical Pharmacology, Graduate School of Pharmaceutical Sciences, The University of Tokyo, 7-3-1 Hongo, Bunkyo-ku, Tokyo 113-0033, Japan. Email: ikegaya@mol.f.u-tokyo.ac.jp

Brain function is supported by a high level of energy metabolism, but the brain itself has no effective energy storage capacity. Its metabolism is mainly oxidative, and the oxygen and nutrients are supplied through cerebral circulation. This energy supply system is protected by cerebral autoregulation, a phenomenon that allows maintenance of constant cerebral blood flow across a wide range of systemic blood pressure levels. Altered autoregulation is believed to result in orthostatic hypotension (Novak *et al.* 1998), syncope (Grubb *et al.* 1991), vascular dementia (Román *et al.* 2002), and Alzheimer's disease (Iadecola, 2004).

Since autoregulation was described by Fog (1937), it has been examined through numerous studies; however, the mechanism involved in this process has not been fully determined, and those that have been proposed are complex, variable and even controversial. The controversy seems to arise, at least in part, from technical limitations. (1) In many studies, blood pressure changes are induced by non-physiologically oppressive conditions, including severe arterial bleeding, hypercapnia, and electric stimulation of baroreflex. These extreme conditions are unlikely to reproduce naturally occurring events in the brain. (2) Most studies have measured the blood flow averaged across many vessels, without separating individual vessels. Such bulk measurement cannot capture the fine-scale regulation occurring in microvessels. (3) Most studies have monitored superficial neocortical vessels on or near the brain surface. The behaviour for these easily accessible shallow vessels may not be a model for the blood flow regulation in deep-brain parenchyma. To our knowledge, there is no study that simultaneously overcame these three limitations.

In this study, we developed a small-diameter objective lens, which allowed us to directly observe deep-brain tissues. In addition, we used pharmacological receptor agonists to induce mild changes in blood pressure. We monitored the capillary flow of individual red blood cells

DOI: 10.1113/jphysiol.2008.163253

(RBCs) in the hippocampus, because this brain region is known to be vulnerable to cerebral ischaemia (Pulsinelli *et al.* 1982). By comparing the hippocampal blood flow to peripheral blood flow, we confirmed that, on average, hippocampal capillaries undergo tight autoregulation, but we also noticed that the degree of autoregulation is different among vessels. These data suggest that rapid autoregulation is based on a local control system that can regulate individual microvessels independently, rather than on a holistic control system at the whole-brain level.

Methods

Experiments were performed with the approval of the animal experiment ethics committee at the University of Tokyo (approval numbers, 19-35 and 19-41) and according to the University of Tokyo guidelines for the care and use of laboratory animals.

Hippocampal vessel reconstruction

Male ICR mice (6 weeks old) were anaesthetized with urethane and perfused transcardially with chilled phosphate-buffered saline (PBS) followed by 4% paraformaldehyde in 0.1 M phosphate buffer (PB; pH 7.4). The brains were removed, fixed with 4% paraformaldehyde overnight at 4°C, and coronally sliced at a thickness of 300 μm using a ZERO-1 vibrating microtome (Dosaka, Osaka, Japan). They were incubated with 100% methanol at 4°C for 30 min, with 2% goat serum in PBS at room temperature for 60 min, and with rat antibody against mouse CD31 (1 : 100; BD Pharmingen, San Diego, CA, USA) at 4°C overnight. They were incubated in 2% goat serum with Alexa 488-labelled anti-rat IgG (1 : 400; Invitrogen, Gaithersburg, MD, USA) and NeuroTrace 530/615 (Invitrogen) for 6 h at room temperature. In some experiments, a clearing procedure was applied to render fixed slices transparent (Dodt *et al.* 2007). The immunostained tissues were further fixed with 4% paraformaldehyde overnight at 4°C and dehydrated in a graded ethanol series (50%, 80%, 99.5% each for 30 min) at room temperature. They were rinsed in 100% hexane for 30 min and then in a clearing solution of benzyl alcohol and benzyl benzoate (1 : 2) for 1 h at room temperature. Hippocampal vessels were imaged with a two-photon laser scanning system using mode-locked Ti:sapphire laser (Mai Tai; Spectra-Physics Inc., Mountain View, CA, USA) and an upright microscope (BX61WI; Olympus, Tokyo, Japan) with a water-immersion objective (20×, XLUMPlanFI/IR, Olympus). Images were three-dimensionally reconstructed using ImageJ (National Institutes of Health, Bethesda, MD, USA). Tissue shrinkage was not corrected.

Blood flow imaging

Male ICR mice (4–10 weeks old) were anaesthetized with urethane (1.5 g kg^{-1}, I.P.) and fixed to a stereotaxic frame. After a small craniotomy (about 2 × 2 mm) of the left hemisphere, the dura was removed for insertion of a custom-made stick-like objective lens (top diameter, 300 μm; bottom diameter, 1050 μm; magnification, 5×; numerical apparatus, 0.13; working distance, 50 μm; Fig. 2*A*). Systemic blood pressure was measured via a catheter inserted into the right carotid artery. Dye and drugs were administered into the tail vein. To visualize blood vessels, blood serum was labelled with 30–250 μl of 1% fluorescein isothiocyanate-labelled dextran (FITC-dextran, 70 kDa) in saline. The dye was repeatedly injected, as required, to minimize photobleaching and dye metabolism. The objective lens was carefully inserted into the dorsal or ventral hippocampus at depths of 1100–4190 μm from the pia surface. We could stably image the same microscopic field for more than 2 h after lens insertion.

Fluorescence images were obtained using an IV100 imaging system with an argon laser (wavelength, 488 nm) and IV10-ASW software (Olympus) with 8× optical zoom. The capillaries of interest were *XT*-scanned along their longitudinal axes. The pixel rate was 10 or 20 μs, and the time resolutions were 0.7–3.4 ms per *X*-scan line. The velocity of each RBC was measured as an angle of its oblique 'shadow' band (Fig. 2*D*). This method is available to capillaries only (diameter, 5–8 μm), due to the vessel diameter relative to RBC size, that is, in larger vessels, a RBC can pass through an out-of-focus depth-of-field, leading to an inappropriate estimation of the RBC flow. After each experiment, the brain was removed and sliced using a vibrating microtome to verify the position of the objective lens. If the tip was placed outside the hippocampus, the data were discarded. Thus, we only used data obtained from 11 out of 18 mice. Using the same optical system, we also monitored the RBC flow in the capillaries of earlobes, which were depilated using a hair remover.

Throughout all experiments, the arterial blood pressure was continuously monitored using a BD P23XL transducer (Ohmeda, Liberty Corner, NJ, USA), an ADC-11 digitizer (Pico Technology Ltd, St Neots, UK), and PicoScope software (Pico Technology), which were synchronized to the imaging system through a SEN-3301 electric stimulator and an SS-403J isolator (Nihon Kohden Corp., Tokyo, Japan). Because this study focused on the rapid effect of blood pressure changes on cerebrovascular blood flow, pH, P_{O_2}, and P_{CO_2} were not monitored. Biologically active reagents, i.e. 2.5 μg kg^{-1} acetylcholine, 0.5 μg kg^{-1} isoproterenol, and 5.0 μg kg^{-1} phenylephrine, were intravenously injected to induce changes in blood pressure.

As the slender objective lens may be physically susceptible to a change in temperature, it was not heated, but the temperature of brain tissues around the lens tip was $29.7 \pm 0.8^{\circ}$C ($n = 3$ mice), which was comparable to that of the brain that received no lens insertion ($29.7 \pm 0.3^{\circ}$C, $n = 3$ mice). Thus, the cooling effect through the inserted lens was negligible.

Results

Uniform alignment of hippocampal vessels

As a first step for *in vivo* imaging, we histologically investigated the hippocampal vasculature. Vessels were immunolabelled with the vascular endothelial cell marker CD31 and reconstructed in Nissl-counterstained hippocampal slices with two-photon laser scanning microscopy.

Because of immunoreactivity and light scattering, thin capillaries could not always be imaged; therefore, we first analysed only larger microvessels (diameter, 10–25 μm). In the stratum radiatum and the pyramidal cell layer, blood vessels tended to run in the direction perpendicular to the pyramidal cell layer, resembling cortical transverse vessels that run perpendicular to the surface of the cerebral cortex, whereas the alignments were more irregular in the stratum lacunosum-moleculare and the dentate molecular layer (Fig. 1*A*, see also Coyle, 1978; Lovick *et al.* 1999). In Fig. 1*B*, the vessel position was projected to a plane cross-sectioned along the CA1 pyramidal cell layer. The mean density of blood vessels in this plane was 372 ± 96 per square millimetre (mean ± S.D., $n = 14$ hippocampi).

To evaluate the unevenness in the spatial distribution of vessels, the coefficient of variation (CV) of the Euclid distance from any given vessel to the nearest one was calculated for each preparation and was compared to the coefficients in the corresponding 100 surrogates, in which the same number of vessels were randomly scattered in the same space and the distance between two vessels was more than 10 μm (Fig. 1*C*). Figure 1*D* shows the cumulative frequency of CV, indicating that the CVs of the real datasets were smaller than those of the surrogates ($n = 14$). Thus, vessels in the pyramidal cell layer are distributed evenly rather than randomly. Given that the

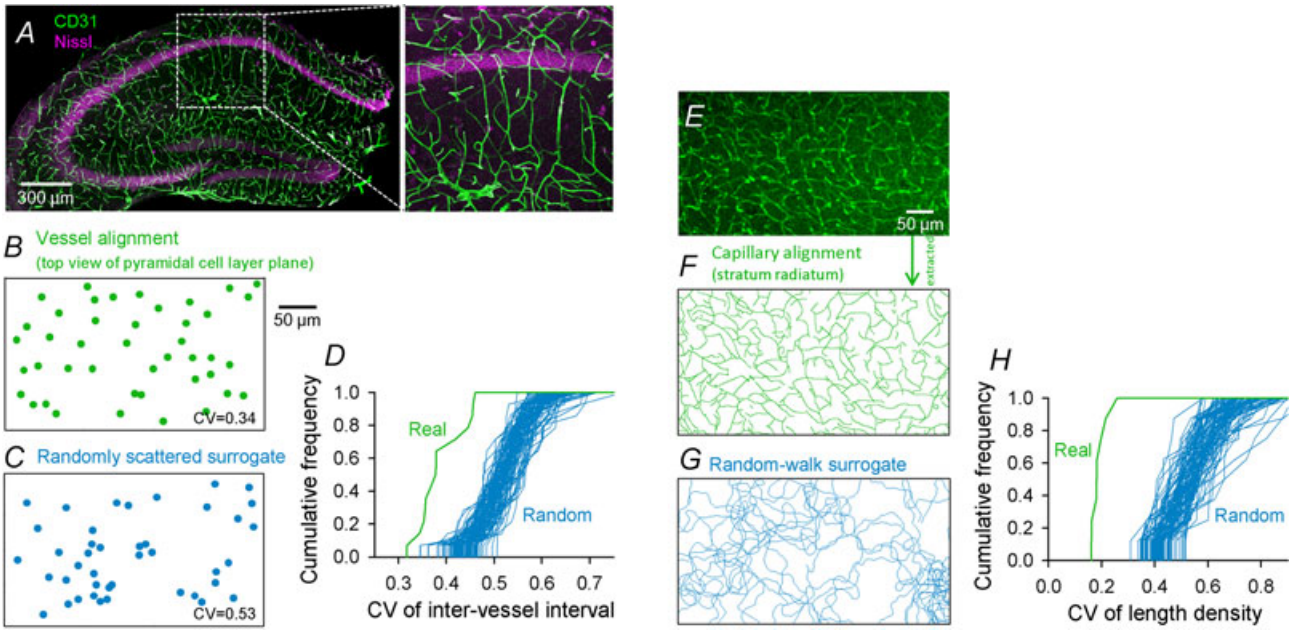

Figure 1. Uniformly aligned blood vessels in the hippocampus
A, representative immunohistochemical image of a hippocampal slice with anti-CD31 antibody, a marker of vascular endothelial cells. Right panel magnifies the region indicated by the white box in left panel. *B*, spatial distribution of vessels across the CA1 pyramidal cell layer (top view cross-section). Each circle represents a single vessel. *C*, the same number of circles as that in *B* was randomly redistributed in the same space. *D*, cumulative frequency of the coefficient of variation (CV) of intervessel intervals, i.e. the distance from a vessel to the closest vessel. The line on the left (green in the online version of the article) indicates the real dataset; the lines on the right (blue in the online version of the article), indicate the 100 surrogates. Note that the real dataset has lower CV than the randomly distributed dataset ($n = 14$ slices). *E*, representative CD31-immunoreactivity of the CA1 stratum radiatum in an optically cleaned hippocampal slice. *F*, eroded traces extracted from *E*. *G*, randomly running trajectories with the same total length as *F*. *H*, cumulative frequency of the CV of the length densities of 100 randomly placed areas (100×100 μm). The real dataset has lower CV than the random-walk ones ($n = 8$ slices).

neuron density in the CA1 pyramidal cell layer was roughly 30 000–40 000 neurons per mm^2 (this value was obtained by stacking three-dimensional images of Nissl-stained cells onto a single plane along the pyramidal cell layer), we estimate that a single transverse vessel feeds about 25 CA1 neurons.

To access small capillaries as well, we next made the fixed tissues optically transparent with a cleaning procedure (Fig. 1*E*). According to Weber *et al.* (2008), we quantified the vascular architecture. The vessel length density in the CA1 stratum radiatum was 376 ± 135 mm mm^{-3} for all vessels (mean ± S.D., $n = 8$ hippocampi). To evaluate the spatial unevenness, 100 boxes (= 100 × 100 μm squares) were randomly placed on a binary vessel image with eroded traces that represent the vessel alignment, and the CV of the length density was calculated across the boxes (Fig. 1*F*). We found again that the CVs of the real datasets were smaller than those of random-walk ($n = 8$, Fig. 1*G* and *H*). The spatial equability of the vessel alignment may allow uniform energy supply to hippocampal neurons.

In vivo imaging of deep-brain regions

To directly access deep-brain regions, we designed a stick-type objective with a tapered tip (Fig. 2*A*). The objective was carefully inserted into the hippocampi of anaesthetized mice (Fig. 2*B*), and the hippocampal vessels were angiographically imaged with intravenously injected FITC-dextran (Fig. 2*C*).

The RBC flow in the hippocampal capillaries was monitored using a single-line scanning approach (Dirnagl *et al.* 1992). RBCs appeared as non-labelled dark interpositions between the FITC-dextran-labelled plasma gaps. In the line-scanned image therefore a pattern of oblique black and white stripes was generated in a space (horizontal axis) *versus* time (vertical axis) plot (Fig. 2*D*), in which the velocity of each RBC was determined by dividing the distance travelled by it (ΔX) by the time needed (ΔT). Under the basal conditions, the RBC velocity was 1.3 ± 0.6 mm s^{-1}, ranging from 0.5 to 2.3 mm s^{-1}, and the number of passing RBCs per second (flux) was 38 ± 15 cells s^{-1} (mean ± S.D., $n = 42$ vessels), ranging from 13 to 70 cells s^{-1}. Neither velocity nor flux was correlated to the capillary diameter (velocity, $R = 0.16$; flux, $R = 0.09$, both $P > 0.1$).

We examined the changes in hippocampal RBC flow corresponding to pharmacologically induced changes in systemic blood pressure. Intravenous acetylcholine and isoproterenol induce hypotension, and phenylephrine induces hypertension. These drugs produced rapid and transient changes in blood pressure within seconds. The mean arterial pressure was 94 ± 15 mmHg under resting conditions (mean ± S.D., $n = 26$); it decreased by 18 ± 4 mmHg after acetylcholine injection ($n = 18$) and by 22 ± 4 mmHg after isoproterenol injection ($n = 14$) and increased by 8 ± 2 mmHg after phenylephrine injection ($n = 13$). In experiments with controls, we monitored the RBC flow in capillaries in the earlobe. We then compared the RBC flow in the hippocampus

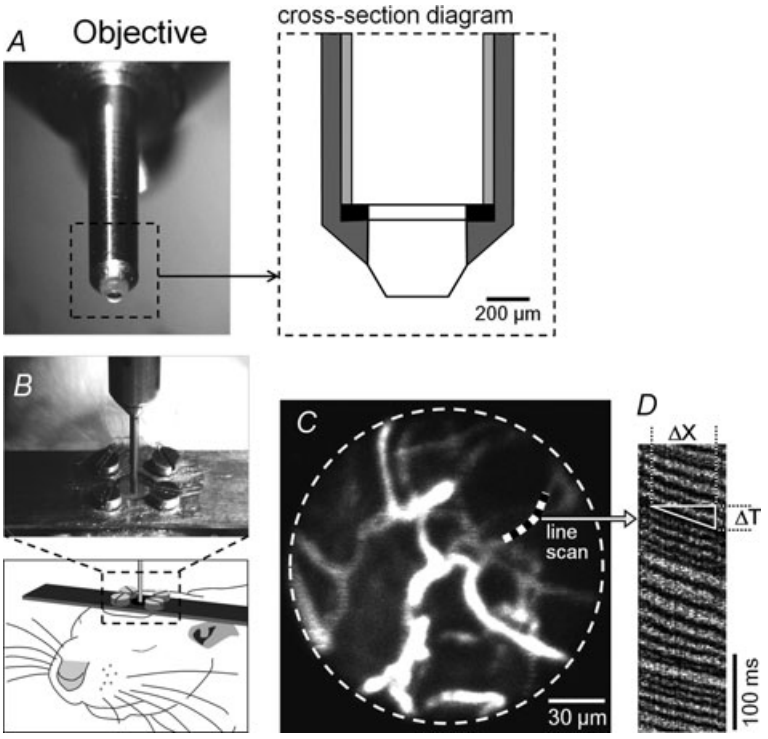

Figure 2. Imaging RBC flow from deep-brain tissue
A, custom-made stick-type objective lens. *B*, FITC-dextran is intravenously injected into a mouse, and the objective lens is directly inserted into the brain parenchyma, 1140–4190 μm beneath the pia surface. *C*, a typical full-scan image of cerebral microvessels. *D*, line-scan image obtained along the line indicated in *C*. Flow of individual RBCs is observed as oblique 'shadow' bands, and the RBC velocity is calculated as the slope $\Delta X/\Delta T$.

(central nervous system) to that in the earlobe (peripheral tissue).

Figure 3 shows representative data of acetylcholine-induced RBC flow changes. The hippocampal RBC velocity or flux did not respond to a change in blood pressure after the acetylcholine injection (Fig. 3*A* and *B*), whereas the RBC flow in the earlobe responded linearly to a decrease in blood pressure (Fig. 3*C* and *D*). The RBC velocity was proportional to RBC flux (Fig. 3*E*).

All data are averaged in Fig. 4*A* and *B*. The overall hippocampal RBC velocity did not significantly change with blood pressure changes ranging from −22 to +8 mmHg (Fig. 4*A*). The RBC velocity in the earlobe responded almost linearly to blood pressure changes (Fig. 4*B*). We then focused on individual capillaries. In each blood vessel, autoregulation was considered if the *P*-value of the regression coefficient was more than 0.05. Among the 45 hippocampal capillaries, 26 capillaries (58%) showed autoregulation, but the remaining did not, that is, they displayed significant changes in RBC flow with changes in blood pressure (Fig. 4*C*), whereas no earlobe capillaries showed autoregulation (Fig. 4*D*). There was no difference in vessel diameters, basal RBC velocity, or basal mean blood pressure between autoregulated and non-autoregulated vessels in the hippocampus (Fig. 4*E*). We observed an autoregulated capillary and a non-autoregulated one in the same microscopic field (Fig. 4*F*). We also compared the degree of autoregulation in the identical vessels between twice drug challenges. Out of six capillaries tested (acetylcholine, $n = 1$; isoproterenol, $n = 3$; phenylephrine, $n = 2$), four exhibited similar levels of autoregulation. However, one capillary did not demonstrate autoregulation after the first injection of acetylcholine, but did after the second (Fig. 4*G*), whereas one demonstrated autoregulation after the first injection of isoproterenol, but did not after the second (data not shown).

Discussion

Using a newly developed slender objective lens, we found that, on average, hippocampal capillaries showed more robust autoregulation than peripheral capillaries.

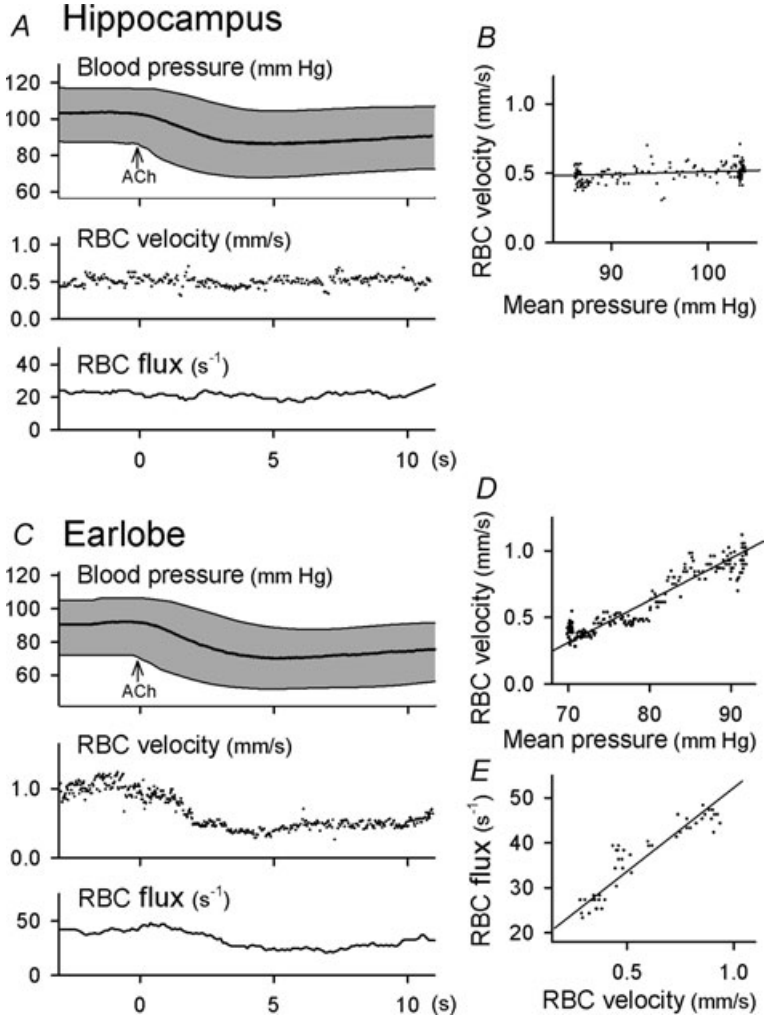

Figure 3. Simultaneous monitoring of carotid blood pressure and RBC flow
A–D, microvessels of the hippocampus (depth, 2130 μm) (*A* and *B*) and earlobe (*C* and *D*) were imaged. Acetylcholine (ACh, 2.5 μg kg^{-1}) was intravenously administered at 0 s to induce a decrease in blood pressure (*A* and *C*). The thick line indicates the mean pressure and the two thin lines, the diastolic and systolic pressures, the area between which is shaded grey (top). The velocity (middle) and flux (bottom) were measured. The RBC velocity in the capillaries of the earlobe responded linearly to blood pressure changes, whereas the hippocampal RBC velocity did not respond. In graphs *B* and *D*, the RBC velocity was plotted *versus* the mean blood pressure. Each point indicates a single RBC. *E*, the RBC flux was linear to the RBC velocity.

This was an expected finding, because the range of pharmacologically induced changes in blood pressure (70–120 mmHg) was within the accepted cerebral autoregulation induction limits (60–150 mmHg). However, the levels of autoregulation were heterogeneous among the blood vessels.

In vivo imaging of deep-brain regions with single-cell resolution

We monitored the dynamics of RBC flow in microvessels located millimetres beneath the pia surface. Historically, deep-brain haemodynamics has been mainly recorded using laser Doppler flowmetry, positron emission tomography, functional magnetic resonance imaging, etc. These techniques, however, can only measure the net change in blood flow, without discriminating the type of vessels. To obtain single-vessel resolution in deep-brain tissues, fluorescence imaging was performed using two-photon laser microscopy (Kleinfeld *et al.* 1998; Helmchen *et al.* 2001; Chaigneau *et al.* 2003; Hutchinson *et al.* 2006). Even with this optical technique, the depth accessed is only hundreds of micrometres. To access deeper tissue, narrow endoscopes that can be intraparenchymally

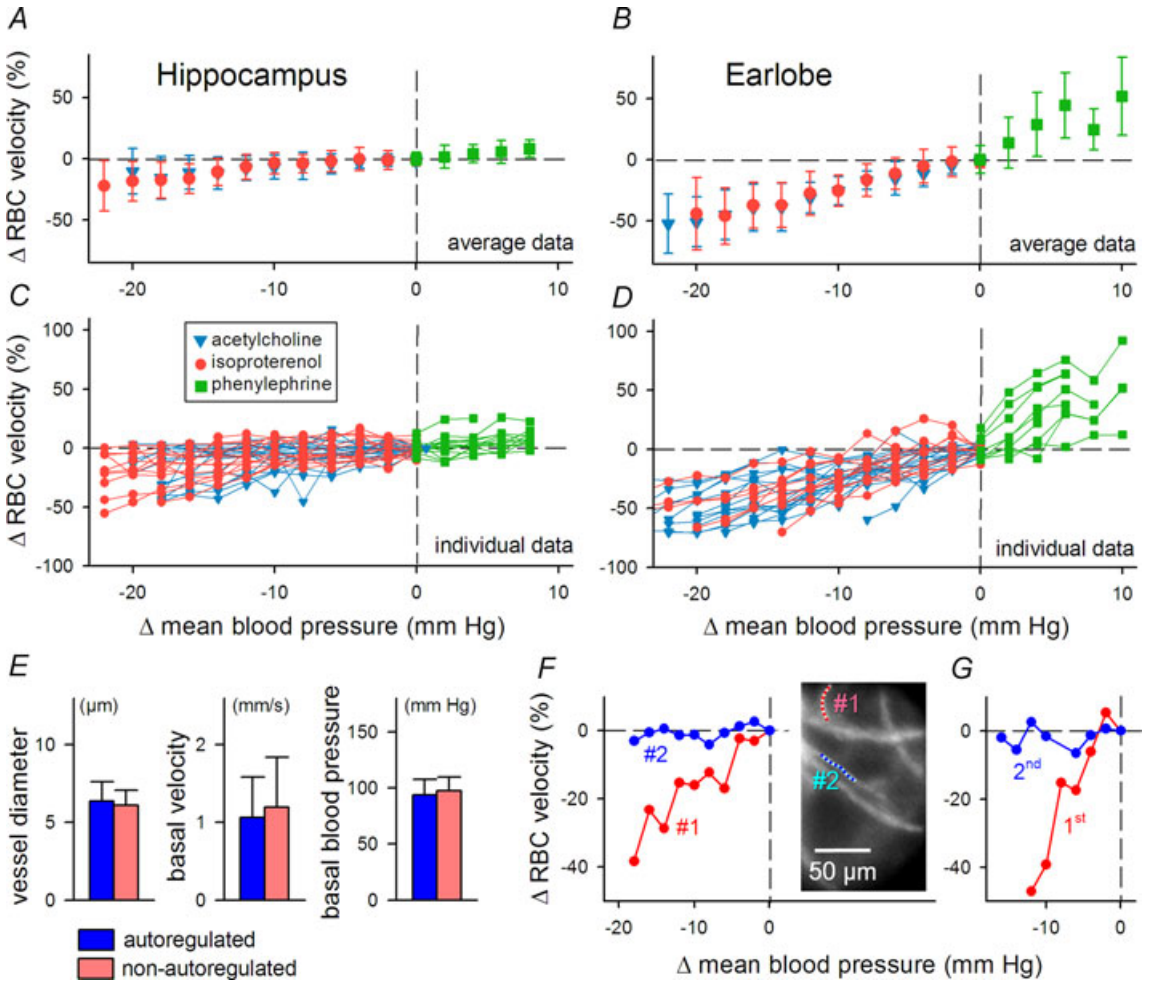

Figure 4. Autoregulation of hippocampal capillaries
RBC velocity of the brain (*A* and *C*) was compared to that of the earlobe (*B* and *D*). Blood pressure changes were pharmacologically induced. Triangles (blue in online version): 2.5 μg kg^{-1} acetylcholine (hippocampus: $n = 18$ vessels from 7 mice, earlobe: $n = 18$ vessels from 4 mice); circles (red in online version): 0.5 μg kg^{-1} isoproterenol (hippocampus: $n = 14$ vessels from 6 mice, earlobe: $n = 11$ vessels from 4 mice); and squares (green in online version): 5.0 μg kg^{-1} phenylephrine (hippocampus: $n = 13$ vessels from 7 mice, earlobe: $n = 10$ vessels from 4 mice). Data are averaged in *A* and *B* (means ± S.D.), whereas all raw data are shown in *C* and *D*. *E*, no difference in vessel diameters, basal RBC velocity, or basal mean blood pressure between autoregulated ($n = 26$) and nonautoregulated vessels ($n = 19$). *F*, monitoring of different vessels in the same field. Closely located vessels showed different levels of autoregulation. *G*, twice injections of acetylcholine. The same vessel showed different levels of autoregulation at different times. The timings of the first and second injections were separated by 3 min.

inserted are required (Jung *et al.* 2004; Levene *et al.* 2004). In the present study, we selected a narrow objective, the top lens of which was tapered to reduce physical damage to tissues. We were able to stably image the RBC flow even at a depth of $> 4000\ \mu$m for hours. The RBC velocity in the hippocampus ($1.3 \pm 0.6\ \mathrm{mm\ s^{-1}}$) was almost equivalent to that in the earlobe ($1.0 \pm 0.3\ \mathrm{mm\ s^{-1}}$) and those in previous reports demonstrating that blood flow at the brain surface ranges between 0.5 and $1.8\ \mathrm{mm\ s^{-1}}$ (Villringer *et al.* 1994; Kleinfeld *et al.* 1998; Seylaz *et al.* 1999; Pinard *et al.* 2000; Chaigneau *et al.* 2003; Hutchinson *et al.* 2006). We thus conclude that tissue damage or compression due to the insertion of the objective lens was minimal.

As reported by Kleinfeld *et al.* (1998), the RBC velocity was proportional to RBC flux (Fig. 3*F*). This indicates that the number of RBCs per unit volume of blood is invariable. Therefore, we adopted the RBC velocity alone as a RBC flow measure.

The mechanism of cerebral autoregulation

We demonstrated the heterogeneity in autoregulation among individual capillaries. This finding is consistent with a study on the superficial part of neocortex (Hudetz, 1997). The heterogeneity is crucial in understanding the mechanism underlying autoregulation. There are mainly two different, but not mutually exclusive, mechanisms, i.e. 'centre'-mediated and local-reflex autoregulation of blood flow. In the centre-mediated autoregulation hypothesis, local blood flow is considered to be under top-down regulation by a remote control centre. For example, cerebral arteries penetrating the brain parenchyma are innervated by subcortical neurons that project into the cortical microvessels and surrounding astrocytes and interneurons (Hamel, 2006). These neurons are mainly located in the raphe nucleus, basal forebrain, thalamus and locus coeruleus, and stimulation of these areas modulates cerebrovascular tone through receptor activation by acetylcholine, serotonin, nitric oxide, etc. Compared to local-reflex autoregulation systems, the centre-mediated systems are more efficient and effective, but they are unable to independently regulate individual vessels (Hamel, 2006). Hence, our observation that vessels did not equally undergo autoregulation favours the local-reflex autoregulation hypothesis, though it does not dispute the centre-mediated autoregulation hypothesis.

With regard to local-reflex autoregulation, mainly two mechanisms have been proposed, i.e. myogenic and metabolic autoregulation. Myogenic autoregulation arises from the direct baroreflex of arteriolar smooth muscle cells in response to changes in cerebral blood pressure, presumably through stretch-induced changes in membrane polarization and a resultant Ca^{2+} increase (Knot & Nelson, 1998). In metabolic autoregulation, arteriolar resistance is modified by diffusible vasoactive metabolites, such as oxygen, carbon dioxide, adenosine and nitric oxide, in response to blood pressure and/or energy depletion (Iadecola, 2004). Metabolic autoregulation requires at least a few seconds to take place. We found, however, that autoregulation is more rapid and robust. Previously, rapid autoregulation was reported to occur in humans (Aaslid *et al.* 1989) and rabbits (Florence & Seylaz, 1992). In these studies, the recovery time constant of autoregulation was estimated to range from 0.2 to 2.4 s (Florence & Seylaz, 1992). In our fine-scale imaging study, no single RBCs in the autoregulated vessels were found to change their velocity against physiologically relevant changes in arterial blood pressure. Given that the RBC flux is tens of cells per second, autoregulation must be implemented, at least, within hundreds of milliseconds. This short response time favours myogenic, rather than metabolic, autoregulation.

In conclusion, we used a slender objective lens to first quantify cerebral autoregulation at the level of individual microvessels in deep-brain regions. The data thus obtained, i.e. the data on heterogeneity and rapid autoregulation, shed light on the mechanisms underlying cerebral autoregulation. Moreover we emphasize that our data provide insight into the link between neuronal activity and haemodynamics. Currently, data of functional haemodynamic imaging techniques are interpreted on the assumption that blood flow and its activity-dependent regulation are not affected by systemic blood pressure because of cerebral autoregulation. However, this assumption does not always hold true, that is, autoregulation could collapse locally. Thus, our study issues a warning against incautious interpretation of brain imaging data.

References

Aaslid R, Lindegaard KF, Sorteberg W & Nornes H (1989). Cerebral auto-regulation dynamics in humans. *Stroke* **20**, 45–52.

Chaigneau E, Oheim M, Audinat E & Charpak S (2003). Two-photon imaging of capillary blood flow in olfactory bulb glomeruli. *Proc Natl Acad Sci U S A* **100**, 13081–13086.

Coyle P (1978). Spatial features of the rat hippocampal vascular system. *Exp Neurol* **58**, 549–561.

Dirnagl U, Villringer A & Einhaupl KM (1992). In-vivo confocal scanning laser microscopy of the cerebral microcirculation. *J Microsc* 165, 147–157.

Dodt HU, Leischner U, Schierloh A, Jährling N, Mauch CP, Deininger K, Deussing JM, Eder M, Zieglgänsberger W & Becker K (2007). Ultramicroscopy: three-dimensional visualization of neuronal networks in the whole mouse brain. *Nat Methods* **4**, 331–336.

Florence G & Seylaz J (1992). Rapid autoregulation of cerebral blood flow: a laser-Doppler flowmetry study. *J Cereb Blood Flow Metab* **12**, 674–680.

Fog M (1937). Cerebral circulation. The reaction of the pial arteries to a fall in blood pressure. *Arch Neurol Psychiatry* **37**, 351–364.

Grubb BP, Gerard G, Roush K, Temesy-Armos P, Montford P, Elliott L, Hahn H & Brewster P (1991). Cerebral vasoconstriction during head-upright tilt-induced vasovagal syncope. A paradoxic and unexpected response. *Circulation* **84**, 1157–1164.

Hamel E (2006). Perivascular nerves and the regulation of cerebrovascular tone. *J Appl Physiol* **100**, 1059–1064.

Helmchen F, Fee MS, Tank DW & Denk W (2001). A miniature head-mounted two-photon microscope high-resolution brain imaging in freely moving animals. *Neuron* **31**, 903–912.

Hudetz AG (1997). Blood flow in the cerebral capillary network: a review emphasizing observations with intravital microscopy. *Microcirculation* **4**, 233–252.

Hutchinson EB, Stefanovic B, Koretsky AP & Silva AC (2006). Spatial flow-volume dissociation of the cerebral microcirculatory response to mild hypercapnia. *Neuroimage* 32, 520–530.

Iadecola C (2004). Neurovascular regulation in the normal brain and in Alzheimer's disease. *Nat Rev Neurosci* **5**, 347–360.

Jung JC, Mehta AD, Aksay E, Stepnoski R & Schnitzer MJ (2004). In vivo mammalian brain imaging using one- and two-photon fluorescence microendoscopy. *J Neurophysiol* **92**, 3121–3133.

Kleinfeld D, Mitra PP, Helmchen F & Denk W (1998). Fluctuations and stimulus-induced changes in blood flow observed in individual capillaries in layers 2 through 4 of rat neocortex. *Proc Natl Acad Sci U S A* **95**, 15741–15746.

Knot HJ & Nelson MT (1998). Regulation of arterial diameter and wall $[Ca^{2+}]$ in cerebral arteries of rat by membrane potential and intravascular pressure. *J Physiol* **508**, 199–209.

Levene MJ, Dombeck DA, Kasischke KA, Molloy RP & Webb WW (2004). *In vivo* multiphoton microscopy of deep brain tissue. *J Neurophysiol* **91**, 1908–1912.

Lovick TA, Brown LA & Key BJ (1999). Neurovascular relationships in hippocampal slices: physiological and anatomical studies of mechanisms underlying flow-metabolism coupling in intraparenchymal microvessels. *Neuroscience* **92**, 47–60.

Novak V, Novak P, Spies JM & Low PA (1998). Autoregulation of cerebral blood flow in orthostatic hypotension. *Stroke* **29**, 104–111.

Pinard E, Engrand N & Seylaz J (2000). Dynamic cerebral microcirculatory changes in transient forebrain ischemia in rats: involvement of type I nitric oxide synthase. *J Cereb Blood Flow Metab* **20**, 1648–1658.

Pulsinelli WA, Brierley JB & Plum F (1982). Temporal profile of neuronal damage in a model of transient forebrain ischemia. *Ann Neurol* **11**, 491–498.

Román GC, Erkinjuntti T, Wallin A, Pantoni L & Chui HC (2002). Subcortical ischaemic vascular dementia. *Lancet Neurol* **1**, 426–436.

Seylaz J, Charbonne R, Nanri K, Von Euw D, Borredon J, Kacem K, Meric P & Pinard E (1999). Dynamic in vivo measurement of erythrocyte velocity and flow in capillaries and of microvessel diameter in the rat brain by confocal laser microscopy. *J Cereb Blood Flow Metab* **19**, 863–870.

Villringer A, Them A, Lindauer U, Einhaupl K & Dirnagl U (1994). Capillary perfusion of the rat brain cortex. An in vivo confocal microscopy study. *Circ Res* 75, 55–62.

Weber B, Keller AL, Reichold J & Logothetis NK (2008). The microvascular system of the striate and extrastriate visual cortex of the macaque. *Cereb Cortex* **18**, 2318–2330.

Acknowledgements

This work was supported in part by a Grant-in-Aid for Science Research on Priority Areas (KAKENHI no. 20019014, Elucidation of neural network function in the brain), a Grant-in-Aid for Science Research (KAKENHI no. 19659013), and The Asahi Glass Foundation.